Acknowledgments

This research work was supported by the National Science Council of Taiwan under Grant NSC-83-0401-E-007-011, and the computational facilities were provided by the National Centre for High-Performance Computing of Taiwan, which the authors gratefully acknowledge. Valuable comments by B. P. Leonard are also appreciated.

References

[1]Leonard, B. P., "A Stable and Accurate Convective Modelling Procedure Based on Quadratic Upstream Interpolation," *Computer Methods in Applied Mechanics and Engineering*, Vol. 19, June 1979, pp. 59–98.

[2]Leonard, B. P., "Simple High Accuracy Resolution Program for Convective Modelling of Discontinuities," *International Journal for Numerical Methods in Fluids*, Vol. 8, Oct. 1988, pp. 1291–1318.

[3]Gaskell, P. H., and Lau, A. K. C., "Curvature-Compensated Convective Transport: SMART, A New Boundedness-Preserving Transport Algorithm," *International Journal for Numerical Methods in Fluids*, Vol. 8, June 1988, pp. 617–641.

[4]Lin, H., and Chieng, C. C., "Characteristic-Based Flux Limiter of an Essentially 3rd-Order Flux-Splitting Method for Hyperbolic Conservation Laws," *International Journal for Numerical Methods in Fluids*, Vol. 13, No. 3, 1991, pp. 287–301.

[5]Harten, A., "On a Class of High Resolution Total-Variation-Stable Finite-Difference Scheme," *Journal of Numerical Analysis*, Vol. 21, No. 1, 1984, pp. 1–23.

[6]Sweby, P. K., "High Resolution Schemes Using Flux Limiters for Hyperbolic Conservation Laws," *Journal of Numerical Analysis*, Vol. 21, No. 5, 1984, pp. 995–1011.

[7]Davis, S. F., "A Simplified TVD Finite Difference Scheme via Artificial Viscosity," *Journal of Scientific and Statistical Computing*, Vol. 8, No. 1, 1987, pp. 1–18.

[8]Yee, H. C., Warming, R. F., and Harten, A., "Implicit Total Variation Diminishing (TVD) Schemes for Steady-State Calculations," *Journal of Computational Physics*, Vol. 57, Feb. 1985, pp. 327–360.

D. S. McRae
Associate Editor

Thin vs Full Navier–Stokes Computation for High-Angle-of-Attack Aerodynamics

D. Degani* and S. W. Marcus†
Technion—Israel Institute of Technology, Haifa 32000, Israel

Introduction

THE forebody of a flight vehicle can be typified by a slender body of revolution. Because such an axisymmetric body is numerically and experimentally tractable, it has been the object of much research over the years. A number of experimenters (e.g., Refs. 1–3) have noted that for such bodies, there is an angle-of-attack range (roughly, from 30 to 65 deg) for which minute imperfections at the tip (e.g., dust accumulation, surface roughness) can cause large asymmetries in the flow pattern. They found that as the angle of attack increases from 30 to 65 deg, the form of the side-force response as a function of the roll angle changes from a continuous, almost periodic variation to a virtually discontinuous square wave, commonly called a bistable variation. For angles of attack beyond 65 deg, the crossflow past the cylindrical part of the body becomes virtually identical to the flow past a two-dimensional cylinder: Vortex shedding occurs, and as the angle of attack tends toward 90 deg the mean side force tends toward zero.

That minute perturbations of body shape can result in finite asymmetries suggests the existence of inherent instabilities in the expected symmetric flow. This is certainly the case as the angle of attack approaches 90 deg since the observed Kármán vortex street beyond the body is well known to be caused by an absolute instability of the symmetric flow: one which would remain even after removal of any perturbation that initiated it. However, in numerical predictions for angles of attack between 30 and 65 deg both for laminar[4–6] and for turbulent[7] flows, the existence of convective instability of the symmetric flow was found. More recent evidence to support the existence of convective instability has been obtained from several experiments.[8,9]

Numerical methods that can simulate the asymmetry phenomenon must account for the fluid viscosity. The degree to which the viscous terms are considered usually affects the complexity and execution time requirements of the computer models. In previous work, we have employed the thin-layer Navier–Stokes (TLNS) model. This model considers only the effect of the viscosity on the flow normal to the body. Objections have been raised regarding the justification for utilizing the TLNS model to study flow asymmetries, because the viscosity effect of the circumferential and streamwise flow components might become important at the high attack angles of interest.

The objective of this work is to test this question by comparing the three-dimensional Beam–Warming thin-layer Navier–Stokes (BW TLNS) algorithm and Beam–Warming full Navier–Stokes (BW FNS) algorithm where all viscous terms are kept. The three-dimensional flux-splitting thin-layer Navier–Stokes (FS TLNS) algorithm will be used as an additional reference.

Numerical Algorithms

The conservation equations of mass, momentum, and energy can be represented in a flux-vector form that is convenient for numerical simulation as

$$\partial_\tau \hat{Q} + \partial_\xi(\hat{F} + \hat{F}_v) + \partial_\eta(\hat{G} + \hat{G}_v) + \partial_\zeta(\hat{H} + \hat{H}_v) = 0 \quad (1)$$

For body-conforming coordinates and attached or mildly separated high-Reynolds number flow, if ζ is the coordinate leading away from the surface, the thin-layer approximation can be applied, which yields[10,11]

$$\partial_\tau \hat{Q} + \partial_\xi \hat{F} + \partial_\eta \hat{G} + \partial_\zeta \hat{H} = Re^{-1}\partial_\zeta \hat{\boldsymbol{S}}^\zeta \quad (2)$$

where only viscous terms in ζ are retained. These have been collected into the vector $\hat{\boldsymbol{S}}^\zeta$, and the nondimensional Reynolds number Re is factored from the viscous flux term. It is Eq. (2) that is solved in the TLNS model.

Flux-Splitting Algorithm

The flux-splitting algorithm[12] may be used to solve Eq. (2). The algorithm is an implicit scheme and uses flux-vector splitting and upwind spatial differencing for the convection terms in one coordinate direction (nominally streamwise). By using upwind differencing for the convective terms in the streamwise direction and central differencing in the other directions, a two-factor implicit approximately factored algorithm is obtained, which is unconditionally stable for a representative model wave equation.

Beam–Warming Algorithms

The FS TLNS algorithm cannot be extended to an FNS solver due to the flux-splitting technique limitation, which does not allow (implicit) consideration of the viscous terms in the streamwise direction. The Beam–Warming algorithm[13] uses central differences in all three directions (ξ, η, ζ) and, therefore, allows the extension of the code to an FNS solver. Equation (1) can be written as

$$\partial_\tau \hat{Q} + \partial_\xi \hat{F} + \partial_\eta \hat{G} + \partial_\zeta \hat{H} = Re^{-1}\big[\partial_\xi(\hat{P}^\xi + \hat{P}^\eta + \hat{P}^\zeta) + \partial_\eta(\hat{R}^\xi + \hat{R}^\eta + \hat{R}^\zeta) + \partial_\zeta(\hat{\boldsymbol{S}}^\xi + \hat{\boldsymbol{S}}^\eta + \hat{\boldsymbol{S}}^\zeta)\big] \quad (3)$$

Received April 6, 1996; revision received Oct. 28, 1996; accepted for publication Nov. 4, 1996; also published in *AIAA Journal on Disc*, Volume 2, Number 2.

*Professor, Mechanical Engineering Department. Associate Fellow AIAA.

†Senior Research Associate, Mechanical Engineering Department.

We refer to this formulation as FNS. If only the $\hat{S}^{\zeta}$ viscous term is retained, the TLNS is obtained. The viscous cross-derivative terms $\partial_{\xi}\hat{P}^{\eta}$, $\partial_{\xi}\hat{P}^{\zeta}$, $\partial_{\eta}\hat{R}^{\xi}$, $\partial_{\eta}\hat{R}^{\zeta}$, $\partial_{\zeta}\hat{S}^{\xi}$, and $\partial_{\zeta}\hat{S}^{\eta}$ cannot be treated implicitly and have been evaluated explicitly as was done for the parabolized Navier–Stokes (PNS) algorithm[14] with no reduction of accuracy.[13] Therefore, the BW FNS algorithm is

$$
\begin{aligned}
&\left[I + h\delta_{\xi}\hat{A}^{n} - h\,Re^{-1}\bar{\delta}_{\xi}J^{-1}\hat{L}^{n}J - D_i|_{\xi}\right]\left[I + h\delta_{\eta}\hat{B}^{n} - h\,Re^{-1}\bar{\delta}_{\eta}J^{-1}\hat{M}^{n}J - D_i|_{\eta}\right]\left[I + h\delta_{\zeta}\hat{C}^{n} - h\,Re^{-1}\bar{\delta}_{\zeta}J^{-1}\hat{N}^{n}J - D_i|_{\zeta}\right]\Delta\hat{Q}^{n} \\
&= -\Delta t\left[\delta_{\xi}(\hat{F}^{n} - \hat{F}_{\infty}) + \delta_{\eta}(\hat{G}^{n} - \hat{G}_{\infty}) + \delta_{\zeta}(\hat{H}^{n} - \hat{H}_{\infty})\right] - \Delta t\,Re^{-1}\left\{\bar{\delta}_{\xi}\left[(\hat{P}^{\xi})^{n} - \hat{P}^{\xi}_{\infty}\right] + \delta_{\xi}\left[(\hat{P}^{\eta})^{n} - \hat{P}^{\eta}_{\infty}\right] + \delta_{\xi}\left[(\hat{P}^{\zeta})^{n} - \hat{P}^{\zeta}_{\infty}\right]\right. \\
&+ \delta_{\eta}\left[(\hat{R}^{\xi})^{n} - \hat{R}^{\xi}_{\infty}\right] + \bar{\delta}_{\eta}\left[(\hat{R}^{\eta})^{n} - \hat{R}^{\eta}_{\infty}\right] + \delta_{\eta}\left[(\hat{R}^{\zeta})^{n} - \hat{R}^{\zeta}_{\infty}\right] + \delta_{\zeta}\left[(\hat{S}^{\xi})^{n} - \hat{S}^{\xi}_{\infty}\right] + \delta_{\zeta}\left[(\hat{S}^{\eta})^{n} - \hat{S}^{\eta}_{\infty}\right] + \bar{\delta}_{\zeta}\left[(\hat{S}^{\zeta})^{n} - \hat{S}^{\zeta}_{\infty}\right] \\
&\left.+ \delta_{\xi}\left[(\Delta\hat{P}^{\eta})^{n-1} + \Delta\hat{P}^{\zeta})^{n-1}\right] + \delta_{\eta}\left[(\Delta\hat{R}^{\xi})^{n-1} + (\Delta\hat{R}^{\zeta})^{n-1}\right] + \delta_{\zeta}\left[(\Delta\hat{S}^{\xi})^{n-1} + \Delta\hat{S}^{\eta})^{n-1}\right]\right\} - D_e(\hat{Q}^{n} - \hat{Q}_{\infty})
\end{aligned}
\tag{4}
$$

where $h = \Delta t$ or $\Delta t/2$ for first- or second-order time accuracy and the freestream base solution (marked with the subscript ∞) is used. Numerical dissipation terms denoted by D_i and D_e in Eq. (4) are employed in all three directions, as combinations of second and fourth differences.

Equation (4) contains all viscous terms and viscous cross terms. The thin-layer viscous model form of the Beam–Warming algorithm can be obtained by neglecting all viscous terms except those solely in the normal ζ direction.

The BW TLNS was found to be about 1.9 times faster than the FS TLNS and as stable as the FS TLNS (142 s/step for $60 \times 100 \times 50$ grid points on an r4400 SGI machine). The BW FNS is about 1.4 times faster than the FS TLNS but is much less stable and so the Courant number must be more restricted (less than 20 in some cases).

Results and Discussion

Computations were carried out at angles of attack $\alpha = 10$, 40, and 60 deg; Mach number $M_{\infty} = 0.2$; and Reynolds number based on body diameter $Re_D = 2.6 \times 10^4$. The body was an ogive cylinder having forebody fineness ratio of 3.5. The computational mesh consisted of $60 \times 100 \times 50$ points in the axial, circumferential, and radial directions, respectively. Grid points were clustered circumferentially and radially to allow enough resolution leeward of the body and in the boundary layer. The results of the three codes (FS TLNS, BW TLNS, and BW FNS), were compared with no disturbance for each angle of attack. Almost the same time history of total normal-force coefficients (less than 0.6% maximum difference for $\alpha = 60$ deg), was observed for each angle of attack with hardly any deviation from symmetry (total side-force coefficients for all cases were less than 10^{-12}).

Figures 1–3 show results for the three angles of attack tested when an upstream disturbance is added. For $\alpha = 10$ deg (Fig. 1), the disturbance was initiated after 134.4 dimensionless time units. As soon as the disturbance is initiated the computed side-force coefficients C_Y (Fig. 1) of the FNS and TLNS codes start to deviate (although these values relative to the normal force are very small due to the low angle of attack). No significant difference was discerned from the normal-force time history. The results of the FS TLNS were almost identical to the results obtained with the BW TLNS code.

A similar behavior was found for $\alpha = 40$ deg (Fig. 2) when the disturbance was turned on after 131.7 dimensionless time units, but the absolute level of C_Y is much larger and growing rapidly with time and, therefore, the absolute deviations between FNS and TLNS results are larger. This behavior was expected because at this angle of attack the flow is already convectively unstable.[4,5] For $\alpha = 60$ deg (Fig. 3) the flow never reached steady state. It is clear from the behavior of the normal-force coefficients that vortex shedding occurred at the back portion of the body and C_N oscillates (Fig. 3a). However, time histories of both codes are the same and C_Y remains zero as long as the disturbance was not turned on (Fig. 3b). When the disturbance was placed asymmetrically upstream of the apex after 112.6 dimensionless time units, the shedding became asymmetric and C_Y showed large oscillations as well. At this point, however, results of the two codes start to deviate. Although the mean is about the same for both the TLNS and FNS, the evolution in time is significantly different. It even appears as if the two solutions oscillate out of phase with each other. It seems obvious that the FNS algorithm picks up different paths, with the differences becoming larger with increasing angle of attack.

Does this imply that for these larger angles of attack, the thin-layer approximation is no longer valid? Upon careful examination of the results, and recalling that all solutions, both symmetric and asymmetric, were obtained with a full grid, another question arises: Why, when the flow is symmetric (i.e., no disturbance added), are there virtually no differences between the FNS and the TLNS representations? Obviously, one may argue that the asymmetric flow creates such a large crossflow that only the FNS algorithm can treat it correctly. But close scrutiny of characteristics of the solutions reveals no significant difference between the results of the different representations. It, therefore, seems more likely that the different codes simply pick up different paths of evolution of the (symmetric) convectively unstable flowfield. The added terms and small differences in programming, which were inconsequential when the symmetric solution was computed, created a slightly different effective disturbance. This new disturbance was enough to start a different

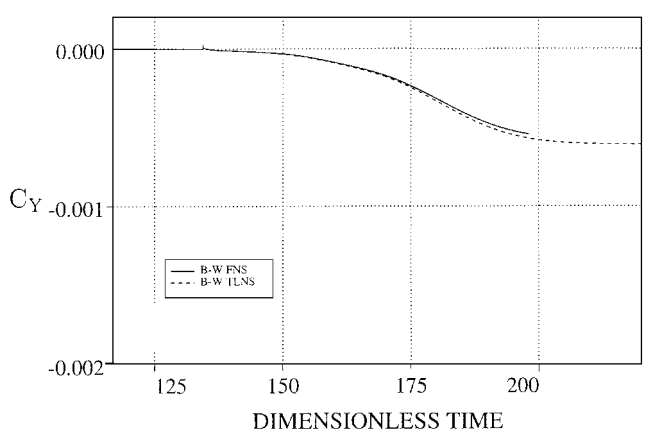

Fig. 1 Time history of side-force coefficient; $\alpha = 10$ deg.

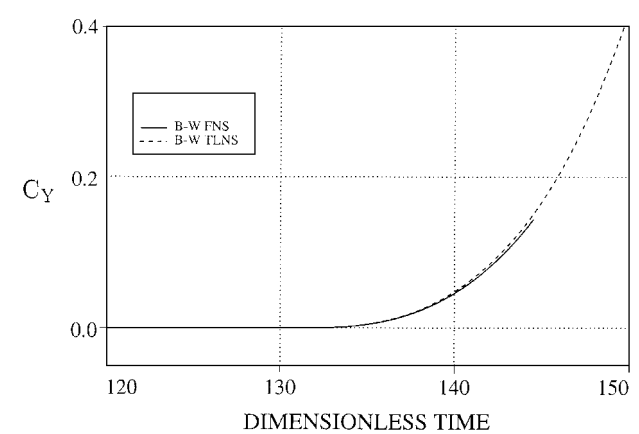

Fig. 2 Time history of side-force coefficient; $\alpha = 40$ deg.

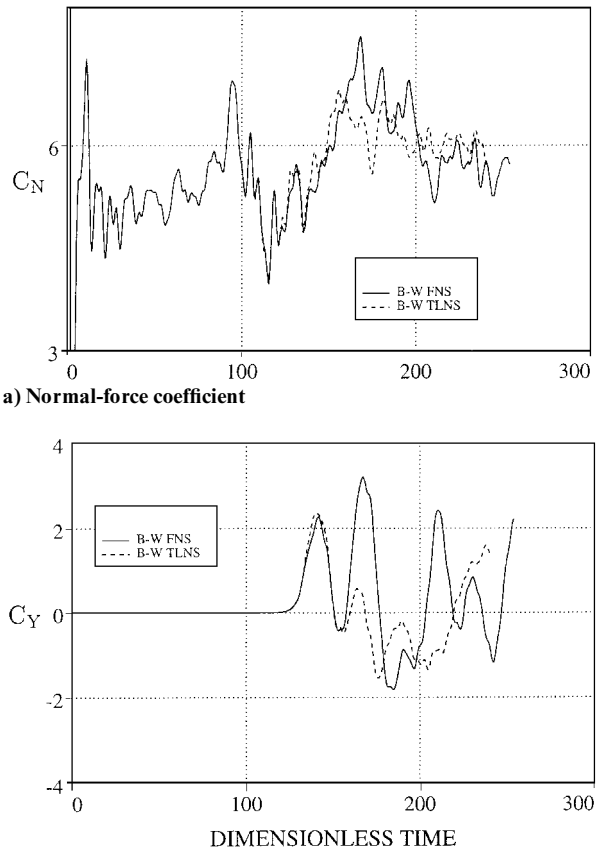

Fig. 3 Time history; $\alpha = 60$ deg.

path of evolution. Such behavior of asymmetric solutions is discussed fully in Ref. 15.

Conclusions

All three codes tested (FS TLNS, BW TLNS, and BW FNS) gave virtually the same results for all three angles of attack (10, 40, and 60 deg) as long as the flow was symmetric.

When the disturbance was placed asymmetrically upstream of the apex of the body, differences between the FNS and TLNS solutions were found. These differences increase as the angle of attack increases.

It is conjectured that the two codes (and also the FS TLNS), pick up different paths of evolution of the (symmetric) convectively unstable flowfield. The added terms and small differences in programming amplified differently the effect of the asymmetric disturbance and acted together as a new, different disturbance.

Acknowledgment

This research was supported by the Israel Science Foundation administered by the Israel Academy of Sciences and Humanities.

References

[1]Hunt, B. L., and Dexter, P. C., "Pressures on a Slender Body at High Angle of Attack in a Very Low Turbulence Level Airstream," AGARD CP 247, Paper 17, 1978.

[2]Lamont, P. J., "Pressures Around an Inclined Ogive Cylinder with Laminar, Transitional, or Turbulent Separation," *AIAA Journal*, Vol. 20, No. 11, 1982, pp. 1492–1499.

[3]Zilliac, G. G., Degani, D., and Tobak, M., "Asymmetric Vortices on a Slender Body of Revolution," *AIAA Journal*, Vol. 29, No. 5, 1991, pp. 560–566.

[4]Degani, D., "Numerical Investigation of the Origin of Vortex Asymmetry," AIAA Paper 90-0593, Jan. 1990.

[5]Degani, D., "Effect of Geometrical Disturbances on Vortex Asymmetry," *AIAA Journal*, Vol. 29, No. 4, 1991, pp. 560–566.

[6]Degani, D., and Schiff, L. B., "Numerical Simulation of the Effect of Spatial Disturbances on Vortex Asymmetry," *AIAA Journal*, Vol. 29, No. 3, 1991, pp. 344–352.

[7]Degani, D., and Levy, Y., "Asymmetric Turbulent Flows over Slender Bodies," *AIAA Journal*, 1992, Vol. 30, No. 9, pp. 2267–2273.

[8]Degani, D., and Tobak, M., "Experimental Study of Controlled Tip Disturbance Effect on Flow Asymmetry," *Physics of Fluids A*, Vol. 4, No. 12, 1992, pp. 2825–2832.

[9]Degani, D., and Tobak, M., "Effect of Upstream Disturbance on Flow Asymmetry," AIAA Paper 92-0408, Jan. 1992.

[10]Baldwin, B. S., and Lomax, H., "Thin Layer Approximation and Algebraic Model for Separated Turbulent Flows," AIAA Paper 78-257, Jan. 1978.

[11]Steger, J. L., "Implicit Finite-Difference Simulation of Flow About Arbitrary Two-Dimensional Geometries," *AIAA Journal*, Vol. 16, No. 7, 1978, pp. 679–686.

[12]Steger, J. L., Ying, S. X., and Schiff, L. B., "A Partially Flux-Split Algorithm for Numerical Simulation of Unsteady Viscous Flows," Proceedings of a Workshop on Computational Fluid Dynamics, Univ. of California, Davis, CA, July 1986.

[13]Beam, R. M., and Warming, R. F., "An Implicit Factored Scheme for Compressible Navier–Stokes Equations," *AIAA Journal*, Vol. 16, No. 6, 1978, pp. 393–402.

[14]Degani, D., and Schiff, L. B., "Computation of Turbulent Supersonic Flows Around Pointed Bodies Having Crossflow Separation," *Journal of Computational Physics*, Vol. 66, No. 1, 1986, pp. 173–196.

[15]Levy, Y., Hesselink, L., and Degani, D., "A Systematic Study of the Correlation Between Geometrical Disturbances and Flow Asymmetries," *AIAA Journal*, Vol. 34, No. 4, 1996, pp. 772–777.

D. S. McRae
Associate Editor

Diamond, Cropped, Delta, and Double-Delta Wing Vortex Breakdown During Dynamic Pitching

Roy Y. Myose,* Boon-Kiat Lee,† Shigeo Hayashibara,* and L. Scott Miller*
Wichita State University, Wichita, Kansas 67260-0044

Introduction

RECENT interest in high angle of attack aerodynamics has refocused attention on delta-shaped wings. Vortices are formed at nonzero angles of attack as flow separates along the leading edges of a delta-shaped wing. Very low pressure is associated with these leading-edge vortices, and they can account for up to 30% of the total lift at moderate angles of attack.[1] For example, lift continues to increase until about a 40-deg angle of attack on a 76-deg swept delta wing.[2] In comparison, symmetric two-dimensional airfoils typically stall out at around a 10- to 15-deg angle of attack. Unfortunately, there are limits to the benefits produced by these delta wing vortices. As the angle of attack is increased, there is a sudden breakdown in vortex structure. This phenomenon, also known as vortex bursting, results in a sudden stagnation in core axial flow and an expansion in radial size.[3] Once this occurs, lift is no longer enhanced aft of the burst point. Thus, the development and subsequent breakdown of leading-edge vortices is crucial to the performance of delta wing aircraft. There have been a number of attempts to control delta wing vortices including the use of blowing,[4,5] suction,[6,7] flaps,[8–10] and canards.[11,12] The reader is referred to Lee and Ho[13] for a more complete review on delta wing vortices.

As the angle of attack is increased on delta wings, the unburst part of the leading-edge vortices becomes shorter. Under dynamic conditions, there is a hysteresis or phase lag in the vortex burst location.

Received Aug. 12, 1996; revision received Dec. 2, 1996; accepted for publication Dec. 9, 1996; also published in *AIAA Journal on Disc*, Volume 2, Number 2.

*Department of Aerospace Engineering. Member AIAA.
†Department of Aerospace Engineering.